A&A 467, 1085–1091 (2007)
DOI: 10.1051/0004-6361:20066816

Astronomy & Astrophysics

New detections of H_2O masers in planetary nebulae and post-AGB stars using the Robledo-70 m antenna⋆

O. Suárez[1], J. F. Gómez[2], and O. Morata[1]

[1] Laboratorio de Astrofísica Espacial y Física Fundamental, INTA, Apartado 50727, 28080 Madrid, Spain
e-mail: olga@laeff.esa.es
[2] Instituto de Astrofísica de Andalucía, CSIC, Apartado 3004, 18080 Granada, Spain

Received 26 November 2006 / Acepted 19 February 2007

ABSTRACT

Aims. We investigated the possible relationship between the evolutionary stage of post-AGB stars and planetary nebulae (PNe) and the presence of water masers in their envelopes
Methods. We have used NASA's 70-m antenna in Robledo de Chavela (Spain) to search for the water maser transition at 22 235.08 MHz, towards a sample of 105 sources with IRAS colour characteristic of post-AGB stars and PNe at declination $>-32^{o}$. 83% of the sources in the sample are post-AGB stars, 15% PNe or PN candidates, while only 2% seem to be HII regions.
Results. We have detected five water masers, of which four are reported for the first time: two in PNe (IRAS 17443−2949 and IRAS 18061−2505), a "water fountain" in a post-AGB star (IRAS 16552−3050), and one in a source previously catalogued as a PN, but whose classification is uncertain (IRAS 17580-3111).
Conclusions. The unexpected detections of water masers in two objects among the small subset of PNe led us to suggest that the PNe harbouring water masers are a special type of massive, rapidly evolving PNe.

Key words. surveys – masers – stars: AGB and post-AGB – ISM: planetary nebulae: general

1. Introduction

Stars with masses between 1 and 8 $M_{\odot}$ start losing their envelope during the Asymptotic Giant Branch (AGB) stage. At this stage, their mass-loss rate can be as high as 10^{-4} $M_{\odot}$ yr^{-1}. When the mass loss stops, the star enters the post-AGB stage (which lasts for between 10^2 and 10^4 years depending on the mass; Blöcker 1995), and its effective temperature increases until it is high enough to ionise the expelled envelope. At this moment the star enters the Planetary Nebula (PN) stage (Kwok 1993).

The circumstellar envelope of the evolved stars provides optimal conditions to pump several types of masers. During the AGB stage, and in O-rich envelopes, SiO, OH and H_2O masers can be pumped (Nyman et al. 1998; Te Lintel Hekkert et al. 1991; Engels & Lewis 1996). These masers are stratified in such a way that SiO masers occupy the innermost part of the envelope, close to the star, water masers are located between 10 and 100 AU from the central star, and OH masers are further away, at $\simeq 10^4$ AU (Reid & Moran 1981). The standard scenario suggests that, when the mass-loss typical of the AGB phase stops, masers disappear sequentially, starting from the innermost ones (Lewis 1989). The timescales for the switching off of masers have been estimated to be $\simeq$10, 100, and 1000 years after the AGB mass-loss stops, for SiO, H_2O, and OH masers, respectively (Gómez et al. 1990), i.e., mostly during the post-AGB phase. Therefore, water masers were thought not to be present during the PNe stage, and only a few of them would show OH emission (Zijlstra et al. 1989). However, Miranda et al. (2001) reported the first confirmed association of a water maser with a PN, in K3-35. Since this detection, only one other PN has been reported to harbour an H_2O maser: IRAS 17347−3139 (de Gregorio-Monsalvo et al. 2004).

Several surveys have been made to search for water masers in evolved stars. Most of them studied to OH/IR and Mira stars (i.e., AGB stars), which have relatively high detection rates (50% in Engels & Lewis 1996). These searches for H_2O masers were based on IRAS colours or fluxes of the target sources (Engels et al. 1984; Zuckerman & Lo 1987; Likkel 1989; Deguchi et al. 1989), whereas others searched for this emission in known OH/IR stars (Engels & Lewis 1996). While some sources with IRAS colours typical of OH/IR and Mira stars are post-AGB stars, no survey so far had focused on the area of the IRAS colour−colour diagram which is mostly populated by post-AGB stars and young PNe, until the very recent one by Deacon et al. (2007). Only a few other works have purposely carried out water maser studies in phases later than the AGB. For example, Engels (2002) performed a monitoring of water masers in four post-AGB stars, and de Gregorio-Monsalvo et al. (2004) searched for water masers in 26 known PNe.

Systematic and sensitive searches for water masers in a large sample of sources including post-AGB stars and PNe are important to properly address whether the presence of water masers in these phases is an evolutionary effect or it is dominated by the characteristics of the central sources. Moreover, the water masers found in these sources can be used as a powerful tool to study these important phases of stellar evolution with an unsurpassable angular resolution ($\lesssim$1 mas), by means of radio interferometric observations.

In this work, we have pursued such a large-scale survey, based on the sources presented in the spectroscopic atlas of post-AGB stars and PNe of Suárez et al. (2006, hereafter SGM). The initial goal of this survey was to find possible relationships

⋆ Tables 1 and 3 are only available in electronic form at http://www.aanda.org

between the evolutionary stage of the post-AGB stars and the presence of water masers in their envelopes. However, the atlas of SGM also included some young PNe, and the detections of water masers in two of these sources (Sect. 4) somewhat changed the initially intended scope. We also note that the survey for water maser emission presented here is one of the most sensitive ones ever carried out toward evolved stars.

In Sect. 2 we describe our selection criteria for the target sources. In Sect. 3 we describe the observations performed. Section 4 contains the results obtained and a description of the detected sources. In Sect. 5 we discuss our results and in Sect. 6 we present our conclusions.

2. Source sample selection criteria

The sample of objects was selected from the atlas of SGM. This atlas was chosen because it contains the largest number of post-AGB stars with spectroscopic classification compiled to date. It also contains some relatively young PNe.

The SGM atlas is composed of IRAS sources located in the region of the IRAS colour−colour diagram populated mainly by post-AGB stars and PNe (van der Veen et al. 1989). The sources in this region are characterised by a range of dust temperatures in their envelopes between 200 K and 80 K, with an expanding radius between 0.01 pc and 0.1 pc.

We have observed all the sources in SGM with $\delta > -32^\circ$ that were classified by these authors as evolved sources, independently of their evolutionary stage. They divide the evolved sources in five groups: PN, post-AGB stars, transition sources (that are evolving between these two categories), peculiar sources (evolved sources with peculiar characteristics), and objects with no optical counterpart. The total amounted to 105 targets. The complete list of observed sources, with their coordinates and classifications according to SGM are listed on Table 1 (in the online version). In this table we also provide other classifications found in the literature for the sources in which no optical counterpart was found by SGM. For the sources with an optical counterpart, we rely on the classification given by SGM based on their optical spectra.

In Fig. 1 we represent the observed sources in the IRAS two-colour diagram showing their evolutionary stage as given by SGM. The IRAS colours [12]−[25] and [25]−[60] are defined in the classical way as:

$$[12] - [25] = -2.5 \log \frac{F_{12\,\mu\mathrm{m}}}{F_{25\,\mu\mathrm{m}}} \quad (1)$$

$$[25] - [60] = -2.5 \log \frac{F_{25\,\mu\mathrm{m}}}{F_{60\,\mu\mathrm{m}}}. \quad (2)$$

The 105 observed targets are initially distributed in evolutionary classes as follows:

- 61 post-AGB stars with optical counterpart;
- 13 transition sources;
- 12 PN with optical counterpart;
- 19 stars without optical counterpart (2 HII regions, 13 post-AGB candidates, 4 PN candidates).

This segregation can be further simplified, if we do not use the information on the presence or not of an optical counterpart. Moreover, we will consider as post-AGB stars all objects classified by SGM as "transition objects", except for IRAS 17347−3139, which seems to be a young PN

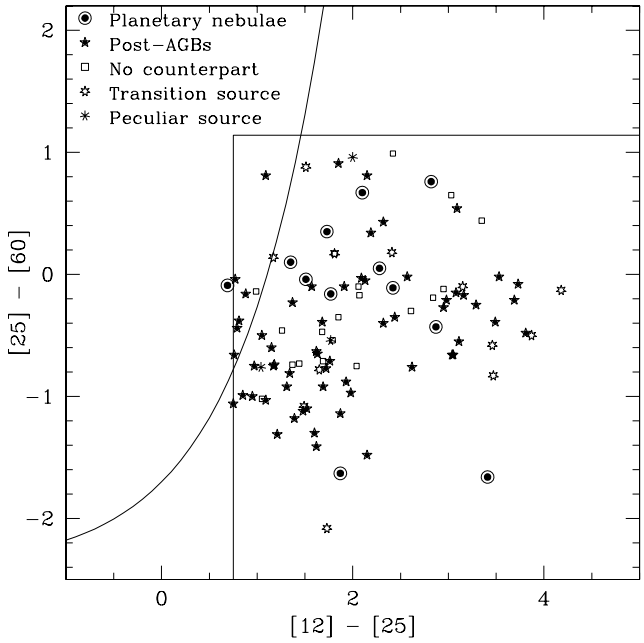

Fig. 1. IRAS colour−colour diagram of the observed sources. The evolutionary classification follows SGM, and the sources in which they did not find an optical counterpart are labelled as such. The two straight lines shown in the diagram delimit the selected colours and the curve is the line modelled by Bedijn (1987) where the AGB stars are located.

(de Gregorio-Monsalvo et al. 2004; Gómez et al. 2005). Note that only two objects in the sample do not seem to be evolved stars.

For the sources without an optical counterpart, we used the classifications given in the literature, although we note that these classifications may not be as reliable as for the ones with observed optical spectra.

With these considerations and caveats, the percentage of sources in each class is:

- 81.9% post-AGB stars;
- 16.2% PNe (bona-fide and candidates);
- 1.9% HII regions.

The observed sample included at least three sources previously confirmed to harbour water masers: the post-AGB starsIRAS 07331+0021 (Engels & Lewis 1996) and IRAS 17392−3020 (Deacon et al. 2007), and the PN IRAS 17347-3139 (de Gregorio-Monsalvo et al. 2004). Han et al. (1998) reported a 4σ detection of 22 Jy toward the post-AGB star IRAS 20406+2953, but Likkel (1989) had not found any maser emission with an rms level of 310 mJy and we did not detect it either (rms $\simeq$ 50 mJy), so this reported detection remains to be confirmed.

3. Observations

We observed the $6_{16} \rightarrow 5_{23}$ transition of the water molecule (rest frequency 22 235.080 MHz), using NASA's 70-m antenna (DSS-63) at Robledo de Chavela (Spain), between October 2004 and March 2006. The 1.3 cm receiver of this antenna comprised a cooled high-electron-mobility transistor (HEMT). The backend used was a 384-channel spectrometer, covering a bandwidth of 16 MHz ($\simeq$216 km s^{-1} with $\simeq$0.6 km s^{-1} resolution). At this frequency, the half-power beamwidth of the telescope is $\simeq$42″.

Table 2. Water maser detections.

IRAS	V_{min}[1] (km s^{-1})	V_{max}[2] (km s^{-1})	V_{peak}[3] (km s^{-1})	S_{max}[4] (Jy)	$\int S_\nu\, d\nu$[5] (Jy km s^{-1})	Date[6]
07331+0021	–104.6	111.2	28.1 ± 0.6	0.21 ± 0.10	0.30 ± 0.21	2006-Jan.-18
16552−3050	–108.2	175.2	−66.8 ± 0.6	1.55 ± 0.23	16.9 ± 1.6	2005-Sep.-11
	–215.9	215.6	88.6 ± 0.6	2.84 ± 0.12	17.8 ± 0.9	2006-Mar.-06
	–215.6	215.4	89.5 ± 0.6	5.54 ± 0.15	28.7 ± 1.5	2006-Apr.-29
17443−2949	–109.1	106.6	−6.3 ± 0.6	8.67 ± 0.18	13.5 ± 0.6	2006-Jan.-09
	–108.0	107.7	−6.4 ± 0.6	10.58 ± 0.17	15.4 ± 0.5	2006-Apr.-12
17580−3111	–162.1	107.7	21.3 ± 0.6	1.09 ± 0.19	1.3 ± 0.4	2006-Apr.-12
18061−2505	–108.0	175.4	57.3 ± 0.6	2.4 ± 0.3	3.7 ± 0.7	2005-Oct.-21
	–107.7	108.1	60.5 ± 0.6	6.95 ± 0.24	8.9 ± 0.7	2006-Jan.-08
	–110.0	105.7	60.9 ± 0.6	3.01 ± 0.16	7.6 ± 0.4	2006-Apr.-12
	–105.8	109.9	57.2 ± 0.6	2.4 ± 0.3	6.1 ± 0.7	2006-May-06

[1] Minimum velocity covered by the observed bandwidth. [2] Maximum velocity covered by the observed bandwidth. [3] Velocity of the emission peak. [4] Flux density of the emission peak. [5] Velocity-integrated flux density of the spectrum. [6] Date of observation.

Spectra were taken in position-switching mode. Only left circular polarisation was processed. System temperatures ranged between 45 and 150 K, depending on elevation and weather conditions, and the total integration time was typically 30 min (on+off). The rms pointing accuracy was better than 10″. The data reduction was performed using the CLASS package, which is part of the GILDAS software.

4. Results

4.1. Survey results

The results of our survey are summarised in Tables 2 and 3 (Table 3 in the online version). We detected water maser emission in five of the 105 observed sources (see Table 2, and Figs. 3 to 7). Four of them were detected in this survey for the first time. They are a post-AGB star: IRAS 16552−3050, a bona fide PN: IRAS 18061−2505, and two PN candidates (without optical counterpart): IRAS 17443−2949, IRAS 17580−3111. However, as discussed below, IRAS 17580−3111 is not likely to be a PN.

Of the sources in our survey previously known to show water maser emission, we detected it in the post-AGB star IRAS 07331+0021, but not in the PN IRAS 17347-3139, nor in the post-AGB stars IRAS 17392−3020 and IRAS 20406+2953.

In Fig. 2 we show their position in the IRAS colour−colour diagram, together with their evolutionary stage. We also include here the position of the other two PNe known to harbour water masers: K3-35, and IRAS 17347−3139. We note that the colours of K3-35 are contaminated by nearby sources, so its position in this diagram is not reliable.

Although it would be very interesting to determine whether the distribution of the detected sources in the IRAS colour−colour diagram differs from the distribution of the complete sample, the small number of H_2O maser detections precludes us from making an statistically significant study. The implementations of the Kolmogorov-Smirnov test to compare two two-dimensional distributions require the number of elements in both groups to be $\gtrsim$10.

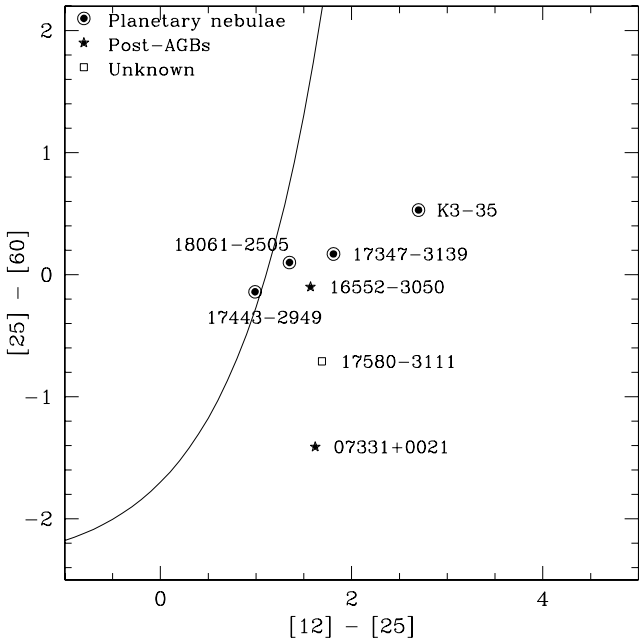

Fig. 2. IRAS colour−colour diagram of the sources in which we detected H_2O maser emission. We also include here the two PNe previously known to harbour water masers. The nature of IRAS 17580−3111 is uncertain, although it was previously classified as a PN (see text).

4.2. Detected post-AGB stars

4.2.1. IRAS 07331+0021

This post-AGB star shows an optical spectrum of K3-5I type (SGM). Its corresponding low temperature (∼4000 K) indicates that the star has probably left the AGB phase very recently. This source presents OH maser emission (Te Lintel Hekkert et al. 1991) with a standard double-peaked profile and mean velocity of ≃27.8 km s^{-1}. The presence of a water maser towards IRAS 07331+0021 was reported by Engels & Lewis (1996), with a peak flux density of 1.2 Jy (0.9 km s^{-1} resolution) at 29.2 km s^{-1}, observed in October 1990.

In our survey, 15 years later, the detected water maser emission was significantly weaker, with one component of ≃0.21 Jy at 28.1 km s^{-1} (Fig. 3), close to the mean velocity of the OH spectrum.

4.2.2. IRAS 16552−3050

IRAS 16552−3050 was first proposed to be a candidate post-AGB star by Preite-Martinez (1988), based on its IRAS colours. A possible optical counterpart of this source was classified by Hu et al. (1993) as a K9III type star, and by SGM as a G0I type. However, recent water maser observations by our group with

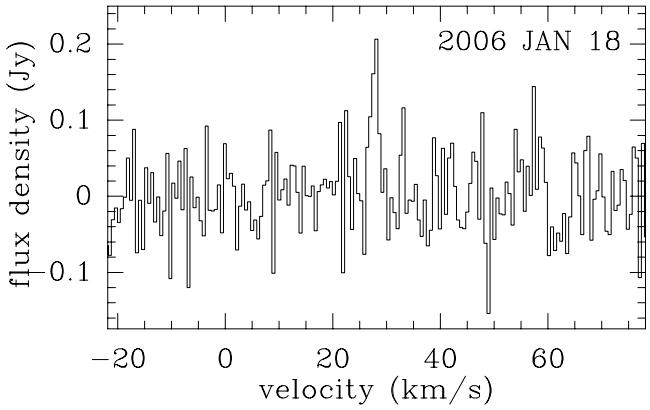

Fig. 3. Water maser spectrum of the post-AGB star IRAS 07331+0021.

the VLA (Suárez et al., in preparation) show that there is no optical source at the position of the water masers. Previous single-dish observations of the OH maser line at 1612 MHz (Te Lintel Hekkert et al. 1998; Hu et al. 1994) did not show any maser emission, with a 1σ rms of 0.2 and 0.1 Jy, respectively.

We detected water maser emission toward IRAS 16552−3050 for the first time on 2005 September 11 (Fig. 4). The spectra show multiple components, with a maximum velocity separation up to $\simeq$170 km s^{-1}. These high velocity separations in maser components indicate that IRAS 16552−3050 is the sixth known source that can be classified as a "water fountain" (Likkel & Morris 1988). The only other known sources of this class are IRAS 16342−3814 (Sahai et al. 1999), IRAS 18043−2116 (Deacon et al. 2007), OH 12.8−0.9 (Boboltz & Marvel 2005), W43A (Imai et al. 2002), and IRAS 19134+2134 (Imai et al. 2004). Water fountains are evolved sources that have just started an episode of bipolar mass loss. Since the mass loss that characterises the Asymptotic Giant Branch (AGB) phase is spherical, in "water fountains" we seem to be witnessing the onset of non-spherical mass loss that may later shape PNe.

The spectra taken at different epochs (Fig. 4) show a high variability in the masers features. In the last epoch (2006 April 29), the components with negative velocities have nearly disappeared.

4.3. Detected PNe and PN candidates

4.3.1. IRAS 17443−2949

This source is one of the objects in the sample of SGM for which no optical counterpart has been found, and that has been classified as a PN. PNe are usually detected at least in the strongest nebular lines, such as [OIII] or in Hα, but in this case the circumstellar envelope still obscures the radiation from the central star, even for the nebular lines. Radio continuum emission in this source was reported by Ratag et al. (1990) [object RZPM 39], with S_ν(6 cm) = 0.9 mJy and a diameter of 3.″4. Zijlstra et al. (1989) found OH maser emission in this PN candidate, and catalogued it as OHPN 10. The distance between the radio continuum and the OH positions are $\simeq$9″, which is smaller than the beam of the OH observations (Zijlstra et al. 1989), and therefore, both emissions probably arise from the same object.

We have found water maser emission (Fig. 5) with a maximum flux density of $\simeq$10 Jy and two well-defined components separated by $\simeq$2 km s^{-1}.

4.3.2. IRAS 18061−2505

This source is a low-excitation bipolar PN, showing two spectacular lobes (SGM). The size of the nebula in the optical (Hα filter) is $\simeq$46″ × 15″. This is the PN with the largest angular size known to harbour water masers. Its radio continuum emission has been detected by Condon & Kaplan (1998) with S(18 cm) = 3.5 ± 1.0 mJy. No OH maser emission was detected in the survey made by Te Lintel Hekkert et al. (1991), with a 1σ rms of 0.1 Jy.

The water maser spectra we obtained with the Robledo antenna show three components (at $\simeq$53.3, 60.5, and 62.0 km s^{-1}) whose relative intensity is very variable. The peak flux density in the spectrum was $\simeq$2−3 Jy in October 2005, April 2006 and May 2006, but it rose to $\simeq$7 Jy in January 2006 (see Fig. 7).

Recent Very Large Array (VLA) observations have confirmed the spatial association of the water maser emission with the central star of the PN (Suárez et al. 2007).

4.4. Detected source with uncertain classification: IRAS 17580−3111

This source was previously classified as a PN, mostly based on the presence of radio continuum emission. Ratag et al. (1990) detected a radio continuum source of S_ν(6 cm) = 2.5 mJy, which they associated with the IRAS source and catalogued this PN candidate as RZPM 45. Although the radio continuum source is within the error box of the IRAS position, the more accurate MSX point source catalog shows an infrared source (MSX6C G359.7798-04.0728) that is $\simeq$30″ away from the radio continuum position, and therefore, their association is unlikely (the position of the MSX source has a 2σ error of $\sim$0.″4).

OH emission was detected in the region by Zijlstra et al. (1989), who catalogued it as OHPN 11. Because of being single-dish observations, it is not possible to determine the location of this emission. No optical counterpart has been found by SGM for this source.

In summary, we believe that the identification of IRAS 17580−3111 as a PN is not well justified. A possibility is that this source is an OH/IR star. However, we also note that its position in the IRAS colour−colour diagram (Fig. 2) is not typical of such type of sources, which tend to lie close to the AGB line modelled by Bedijn (1987). Our speculation is that the source is a post-AGB star, given its position in the diagram, although this suggestion need confirmation.

We have detected water maser emission (Fig. 6) towards this source with a flux density of $\simeq$1.1 Jy. The spectrum is dominated by a component at $\simeq$21.3 km s^{-1}, although a weaker one at $\simeq$19.5 km s^{-1} also seems to be present. We note that the radio continuum source reported by Ratag et al. (1990) falls outside the Robledo beam, which further reinforces our suggestion that the pumping source of the maser emission is not likely to be a planetary nebula.

5. Discussion

5.1. Characteristics of the detected sources

The two post-AGB stars in our survey found to harbour water masers do not seem to have much in common. IRAS 07331+0021 could be a low-mass star slowly evolving away from the AGB stage. Its position in the IRAS colour−colour diagram and its low temperature support this hypothesis. IRAS 16552−3050 belongs to the "water fountain" type. These objects evolve rapidly in the post-AGB stage and show a fast stellar wind that may shape the future PNe.

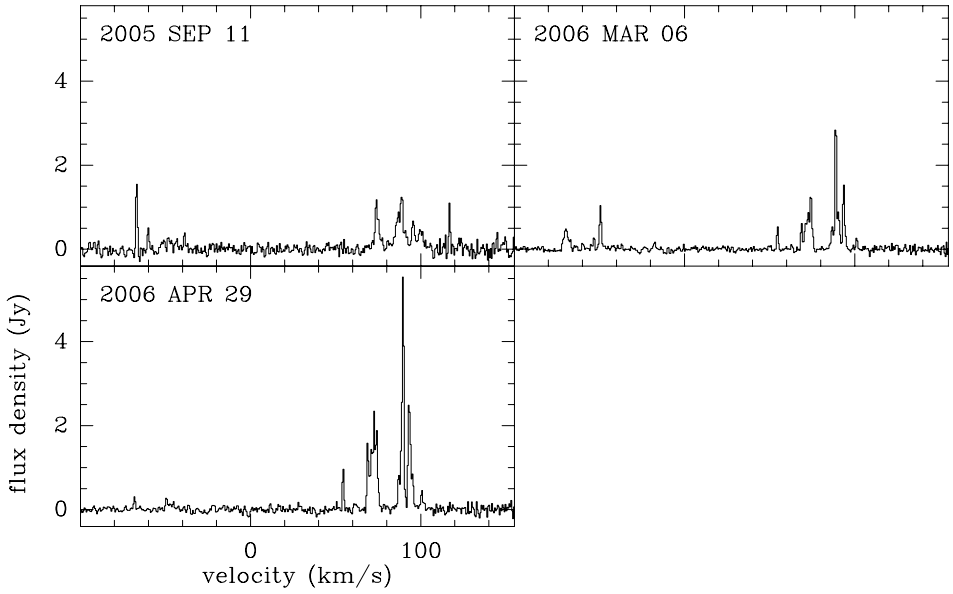

Fig. 4. Water maser spectra of the post-AGB star IRAS 16552−3050.

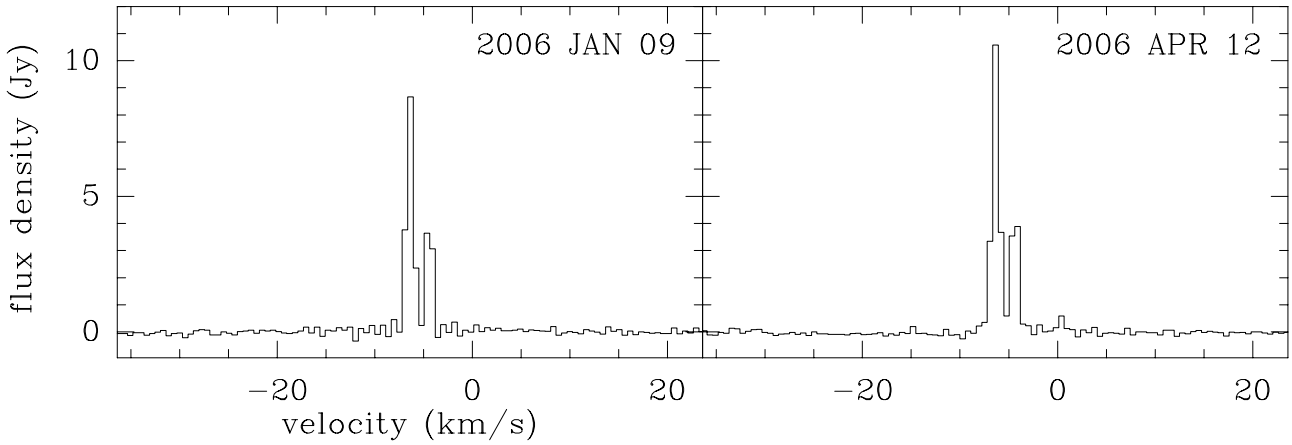

Fig. 5. Water maser spectra of the PN IRAS 17443−2949.

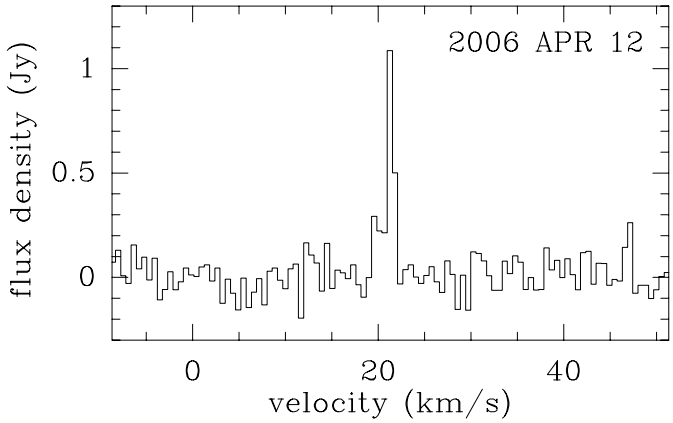

Fig. 6. Water maser spectrum of the PN IRAS 17580−3111.

With our two new detections of water masers in PNe and PN candidates (hereafter referred to as H_2O-PNe), there are now four such objects known, and we can start looking for common patterns, although most of these objects have not been well studied. Two of the four known H_2O-PNe are strongly obscured: IRAS 17443−2949 [OHPN 10] has not been detected in the optical range, while IRAS 17347−3139 [OHPN 5] was only detected in [S III] at λ9069 Å by SGM, but it does not show any stellar or nebular emission at shorter wavelengths. The other two PNe with known water masers are optically visible, although K3−35 is a compact PNe (Miranda et al. 1998). IRAS 18061−2505 is a somewhat "classical" PN, showing two large bipolar lobes (SGM).

In the three cases for which the PN status has been confirmed, and their morphology determined (K3-35, IRAS 17347−3139, IRAS 18061−2505), the objects are bipolar. Moreover, all H_2O-PNe, except for IRAS 18061−2505, show OH maser emission (see Sect. 4).

With so few cases of known H_2O-PNe, it is difficult to draw firm conclusions, although our data seem to suggest that H_2O masers might be favoured in obscured, bipolar PNe, which also show OH maser emission. The characteristics of these H_2O-PNe suggest that they are very young and relatively massive PNe, as discussed in Gómez et al. (2005) for IRAS 17347−3139, which seems to be a good example of this

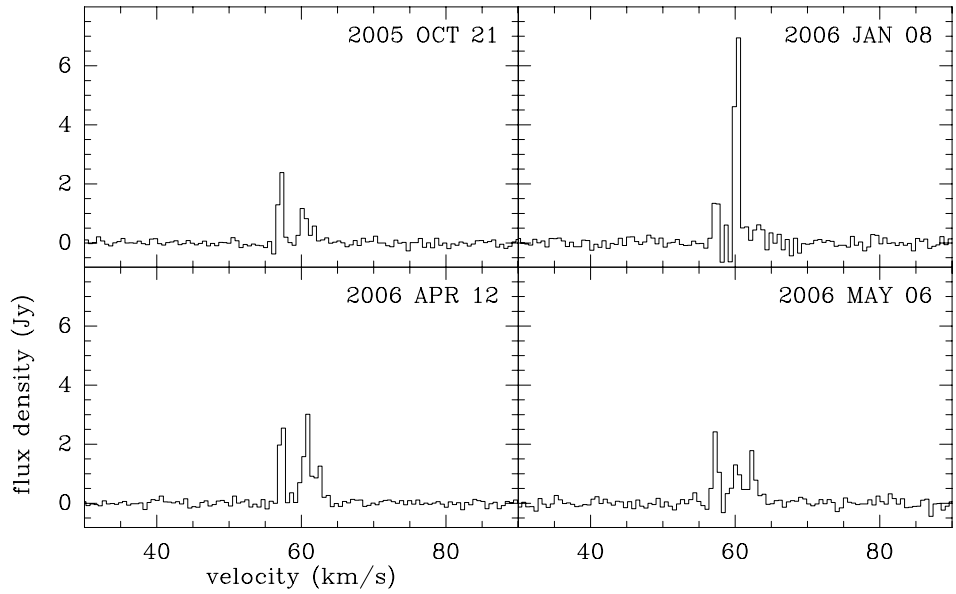

Fig. 7. Water maser spectra of the PN IRAS 18061−2505.

special type of source. More studies on the physical properties of these still poorly known PNe in which we have detected water maser emission would help to confirm the trends that have been suggested here.

5.2. Detection rates and completeness of the sample observed

It is surprising that our detection rate of water masers is ≃5 times larger in objects classified as PNe than in post-AGB stars, and this seems to contradict the simple scenario of masers disappearing as stars evolve. The most straightforward conclusion from our detection rates would be that there is a process that powers water masers in young PN, and that was not at work in the immediately previous phase. However, before reaching this or any conclusion based on detection rates for each category of sources, we first have to analyse the completeness of the sample observed and any possible biases that may be present in it.

The sample in SGM aimed to be complete in the selection of post-AGB stars with optical counterparts. Sources that were not likely to have optical counterparts were excluded from their catalogue. Since our original goal in this paper was to study the incidence and evolution of water masers in post-AGB stars, the SGM catalogue was an appropriate choice, because it included the largest number of post-AGB stars with reliable classification. As it was actively avoided by SGM, the subset of the objects for which no counterpart was found is not complete. Regarding PNe, the SGM sample is further biased to favour faint, low excitation, not well-known PNe. Unfortunately, in two out of four cases, water masers were found in optically obscured PNe, exactly the type of source for which the sample is least complete.

The incompleteness of the samples of PNe and objects without optical counterpart in our survey, as well as the still uncertain nature of the most obscured objects, prevent us from extracting definitive statistical conclusions from the detection rate results, however, we can still speculate about possible scenarios for the presence of water masers in PNe.

5.3. Position of the detected sources in the IRAS colour–colour diagram

In Fig. 2 we show the position of the detected sources in the IRAS colour−colour diagram. We also included the known H_2O-PNe IRAS 17347−3139 and K3-35, although the latter does not have reliable colours (see Sect. 4). Even though the location of a star in this diagram does not directly define its evolutionary status, all the stars located in the same region share common characteristics. In this case, we do not find any water maser detection with [12]−[25] > 2 or [25]−[60] > 0.2, except for K3-35.

The region of the diagram in which our detections lie is characterised by relatively hot envelopes (or envelopes close to the central star). The stars located here are those that have recently left the AGB stage (see Bedijn 1987; Blöcker 1995). If they already have high temperatures, this means that they have evolved very fast, which implies a high mass. This is the case for all the PNe located in this region.

5.4. Possible scenarios for the presence of water masers in PNe

The detection of two water masers towards objects classified as PNe (thus increasing the number of known H_2O-PNe to four sources) is somewhat surprising if we assume a linear scenario of masers disappearing after the AGB mass-loss stops (Lewis 1989; Gómez et al. 1990). Even more surprising in this framework could be that the detection rate in PNe is 5 times higher than in the previous post-AGB phase. Our results are more easily explained if the water masers that have been detected in PNe are not the remnants of the masers pumped by the spherical AGB wind, but they correspond to a later episode of non-spherical mass loss.

Lewis (1989) pointed out that his evolutionary sequence for the sequential disappearance of SiO, OH, and H_2O masers was valid for the spherical mass-loss phase only. The discovery of "water fountain" post-AGB stars, in which OH and H_2O masers trace collimated ejections with short dynamical ages is a compelling piece of evidence of a later phase with non-spherical winds that can pump water masers (see Engels 2002;

Deacon et al. 2007). Our suggestion is that water masers found in PNe are related to this phase of non-spherical winds, and that their precursors in the post-AGB phase could show water masers of the "water fountain" type or similar ones at somewhat lower velocities. These suggestions are supported by the fact that H_2O-PN tend to have a bipolar morphology, and that some of the water maser components in K3-35 have been found at the tips of the bipolar nebula (Miranda et al. 2001).

The somewhat higher detection rate we found in PNe of our sample over that in post-AGB stars can be explained if the pumping of water masers by non-spherical winds is not a general phase that most sources undergo, but they pertain to a particular class of evolved stars. As we pointed out in Sect. 5.2, our survey was not complete for evolved sources without optical counterparts. If the precursors of H_2O-PN are actually post-AGB stars without optical counterparts, they would have been left out of our observations, and therefore, the detection rates of water masers in post-AGB and PNe in our survey are not directly comparable.

We speculate that these H_2O-PNe could represent a different class of PNe, more massive than the classical ones, whose evolution through the post-AGB stage is so rapid that they still maintain their thick AGB envelope when they reach the PN stage. This envelope would mask the UV radiation from the central star, preventing the water molecules from being destroyed, while it would also tend to obscure their emission in the optical.

If this scenario is true, we should be able to find water maser emission in the precursors of these obscured and massive PNe. However, the evolution of these sources would be so rapid during the post-AGB stage that few objects would be found in this stage. Following Blöcker (1995), a star with 1 $M_\odot$ will need 8.3×10^3 yr to reach a temperature of 25 000 K, while a star with 5 $M_\odot$ will only need 100 yr to reach the same temperature. Moreover, these objects would not be visible in the optical, and their identification as post-AGB stars would be difficult.

As we have already discussed, the sample of observed objects was not complete in the selection of obscured post-AGB stars. To confirm or reject our suggestions, a survey for water masers in a complete set of optically obscured post-AGB stars should be carried out.

6. Conclusions

We have performed a survey for water masers in a sample of 105 evolved stars selected from the SGM atlas, using the Robledo 70-m antenna.

We have detected water masers in five sources, four of which are new detections. Our new detections comprise one post-AGB "water fountain" source (IRAS 16552−3050), two PNe harbouring water masers (IRAS 17443−2949, and IRAS 18061−2505), and a source of uncertain nature, previously classified as a PN (IRAS 17580−3111).

We suggest the possibility that PNe with water maser emission are a special class of massive, rapidly evolving PNe that are able to maintain a thick envelope, and that water masers in these sources are related to processes of non-spherical mass-loss, rather than being the remnant of water masers pumped by spherical winds in the AGB phase.

Acknowledgements. We would like to thank our referee, Dr. Dieter Engels, for his careful and useful review, and Dr. Jessica Chapman for her comments on the manuscript and for sharing with us some of her results before publication. This paper is based on observations taken during "host-country" allocated time at Robledo de Chavela. This time is managed by the LAEFF of INTA, under agreement with NASA/INSA. The authors would also like to thank the Radio Astronomy Department and the operation staff at MDSCC for their support during our observations. J.F.G. and O.M. acknowledge support from MEC (Spain) grant AYA 2005-08523-C03 (co-funded by FEDER funds), O.S. acknowledges support from MEC (Spain) grant AYA 2003-09499. O.S. and J.F.G. are also supported by Junta de Andalucía (grants FQM-1747 and TIC-126).

References

Bedijn, P. J. 1987, A&A, 186, 136
Blöcker, T. 1995, A&A, 299, 755
Boboltz, D. A., & Marvel, K. B. 2005, ApJ, 627, L45
Bronfman, L., Nyman, L.-A., & May, J. 1996, A&AS, 115, 81
Condon, J. J., & Kaplan, D. L. 1998, ApJS, 117, 361
de Gregorio-Monsalvo, I., Gómez, Y., Anglada, G., et al. 2004, ApJ, 601, 921
Deacon, R. M., Chapman, J. M., Green, A. J., & Sevenster, M. N. 2007, ApJ, in press
Deguchi, S., Nakada, Y., & Forster, J. R. 1989, MNRAS, 239, 825
Engels, D. 2002, A&A, 388, 252
Engels, D., & Lewis, B. M. 1996, A&AS, 116, 117
Engels, D., Habing, H. J., Olnon, F. M., Schmid-Burgk, J., & Walmsley, C. M. 1984, A&A, 140, L9
García-Lario, P., Manchado, A., Pych, W., & Pottasch, S. R. 1997, A&AS, 126, 479
Gómez, J. F., de Gregorio-Monsalvo, I., Lovell, J. E. J., et al. 2005, MNRAS, 936
Gómez, Y., Moran, J. M., & Rodríguez, L. F. 1990, Rev. Mex. Astron. Astrofis., 20, 55
Han, F., Mao, R. Q., Lu, J., et al. 1998, A&AS, 127, 181
Hu, J. Y., Slijkhuis, S., de Jong, T., & Jiang, B. W. 1993, A&AS, 100, 413
Hu, J. Y., Te Lintel Hekkert, P., Slijkhuis, F., et al. 1994, A&AS, 103, 301
Imai, H., Obara, K., Diamond, P. J., Omodaka, T., & Sasao, T. 2002, Nature, 417, 829
Imai, H., Morris, M., Sahai, R., Hachisuka, K., & Azzollini, F. J. R. 2004, A&A, 420, 265
Kerber, F., Mignani, R. P., Guglielmetti, F., & Wicenec, A. 2003, A&A, 408, 1029
Kwok, S. 1993, ARA&A, 31, 63
Lewis, B. M. 1989, ApJ, 338, 234
Likkel, L. 1989, ApJ, 344, 350
Likkel, L., & Morris, M. 1988, ApJ, 329, 914
Miranda, L. F., Torrelles, J. M., Guerrero, M. A., Aaquist, O. B., & Eiroa, C. 1998, MNRAS, 298, 243
Miranda, L. F., Gómez, Y., Anglada, G., & Torrelles, J. M. 2001, Nature, 414, 284
Nyman, L.-A., Hall, P. J., & Olofsson, H. 1998, A&AS, 127, 185
Persi, P., Palagi, F., & Felli, M. 1994, A&A, 291, 577
Preite-Martinez, A. 1988, A&AS, 76, 317
Ratag, M. A., Pottasch, S. R., Zijlstra, A. A., & Menzies, J. 1990, A&A, 233, 181
Reid, M. J., & Moran, J. M. 1981, ARA&A, 19, 231
Sahai, R., Te Lintel Hekkert, P., Morris, M., Zijlstra, A., & Likkel, L. 1999, ApJ, 514, L115
Suárez, O., García-Lario, P., Manchado, A., et al. 2006, A&A, 458, 173
Suárez, O., Gómez, J. F., & Morata, O. 2007, ApJ, submitted
Te Lintel Hekkert, P., Caswell, J. L., Habing, H. J., et al. 1991, A&AS, 90, 327
Te Lintel Hekkert, P., Caswell, J. L., Habing, H. J., Haynes, R. F., & Norris, R. P. 1998, VizieR Online Data Catalog, 409, 327
Ueta, T., Meixner, M., Dayal, A., et al. 2001, ApJ, 548, 1020
van de Steene, G. C., & Pottasch, S. R. 1995, A&A, 299, 238
van der Veen, W. E. C. J., Habing, H. J., & Geballe, T. R. 1989, A&A, 226, 108
Zijlstra, A. A., Te Lintel Hekkert, P., Pottasch, S. R., et al. 1989, A&A, 217, 157
Zuckerman, B., & Lo, K. Y. 1987, A&A, 173, 263

Online Material

Table 1. List of observed sources. Classification as in Suárez et al. (2006) is also listed. Other classifications in the literature are given for objects listed as peculiar or without an optical counterpart in Suárez et al. (2006).

IRAS	RA (J2000)	Dec (J2000)	Classification Suárez et al. (2006)	Other classification
00509+6623	00:54:07.7	+66:40:13	No counterpart	Post-AGB cand.[1]
01005+7910	01:04:45.5	+79:26:46	Post-AGB	
01259+6823	01:29:33.4	+68:39:17	Post-AGB	
02143+5852	02:17:57.8	+59:05:52	Post-AGB	
04137+7016	04:19:07.7	+70:23:23	No counterpart	Post-AGB cand.[2]
04296+3429	04:32:57.0	+34:36:12	Post-AGB	
05089+0459	05:11:36.2	+05:03:26	Post-AGB	
05113+1347	05:14:07.8	+13:50:28	Post-AGB	
05341+0852	05:36:55.1	+08:54:09	Post-AGB	
05381+1012	05:40:57.1	+10:14:25	Post-AGB	
05471+2351	05:50:13.9	+23:52:18	Peculiar	BQ[ ][3]
05573+3156	06:00:33.4	+31:56:44	No counterpart	HII region[4]
06499+0145	06:52:28.2	+01:42:12	No counterpart	HII region[5]
06518−1041	06:54:13.4	−10:45:38	PN	
06530−0213	06:55:31.8	−02:17:28	Post-AGB	
06556+1623	06:58:30.4	+16:19:26	Peculiar	BQ[ ][3]
07134+1005	07:16:10.3	+09:59:48	Post-AGB	
07227−1320	07:25:03.1	−13:26:20	Post-AGB	
07253−2001	07:27:33.0	−20:07:19	Post-AGB	
07331+0021	07:35:41.2	+00:14:58	Post-AGB	
07430+1115	07:45:51.4	+11:08:19	Post-AGB	
08005−2356	08:02:40.7	−24:04:43	Post-AGB	
08187−1905	08:20:57.1	−19:15:03	Post-AGB	
16476−1122	16:50:24.3	−11:27:58	Post-AGB	
16552−3050	16:58:27.8	−30:55:06	Post-AGB	
16559−2957	16:59:08.2	−30:01:40	No counterpart	Post-AGB[6]
17074−1845	17:10:24.2	−18:49:01	Transition	
17086−2403	17:11:38.9	−24:07:33	Transition	
17106−3046	17:13:51.8	−30:49:41	Post-AGB	
17195−2710	17:22:43.6	−27:13:37	Post-AGB	
17203−1534	17:23:11.9	−15:37:15	Post-AGB	
17223−2659	17:25:25.2	−27:02:03	Post-AGB	
17253−2831	17:28:33.0	−28:33:26	Post-AGB	
17269−2235	17:29:58.7	−22:37:44	No counterpart	PN[7]
17291−2402	17:32:12.8	−24:05:00	Transition	
17317−2743	17:34:53.3	−27:45:11	Post-AGB	
17332−2215	17:36:17.7	−22:17:25	Post-AGB	
17347−3139	17:38:00.6	−31:40:55	Transition	
17364−1238	17:39:16.9	−12:40:30	Post-AGB	
17371−2747	17:40:23.3	−27:49:12	PN	
17376−2040	17:40:38.6	−20:41:53	Post-AGB	
17381−1616	17:40:59.8	−16:17:59	PN	
17388−2203	17:41:49.0	−22:05:16	Post-AGB	
17392−3020	17:42:30.4	−30:22:11	Post-AGB	
17395−0841	17:42:14.4	−08:43:19	PN	
17423−1755	17:45:14.2	−17:56:47	Transition	
17436+5003	17:44:55.5	+50:02:39	Post-AGB	
17441−2411	17:47:13.5	−24:12:51	Post-AGB	
17443−2949	17:47:35.3	−29:50:57	No counterpart	PN[8]
17466−3031	17:49:52.5	−30:33:02	Transition	
17488−1741	17:51:48.9	−17:42:26	Post-AGB	
17514−1555	17:54:21.1	−15:55:52	PN	
17516−2526	17:54:43.4	−25:26:28	Post-AGB	
17542−0603	17:56:56.0	−06:04:10	Post-AGB	

Table 1. continued.

IRAS	RA (J2000)	Dec (J2000)	Classification [SGM]	Other classification
17576−2653	18:00:49.6	−26:53:13	Post-AGB	
17579−3121	18:01:12.8	−31:22:00	Post-AGB	
17580−3111	18:01:19.6	−31:11:22	No counterpart	PN[8]
17582−2619	18:01:21.6	−26:19:37	No counterpart	Post-AGB[9]
17597−1442	18:02:38.3	−14:42:03	PN	
18044−1303	18:07:15.3	−13:03:29	Post-AGB	
18061−2505	18:09:12.4	−25:04:34	PN	
18062+2410	18:08:20.1	+24:10:43	Transition	
18075−0924	18:10:15.1	−09:23:35	Post-AGB	
18186−0833	18:21:21.1	−08:31:42	PN	
18246−1032	18:27:24.0	−10:30:24	No counterpart	Non-var OH/IR[9]
18401−1109	18:42:57.1	−11:06:53	PN	
18415−2100	18:44:32.0	−20:57:13	Peculiar	RCrB type
18420−0512	18:44:41.7	−05:09:17	Post-AGB	
18442−1144	18:47:04.0	−11:41:12	Transition	
18520+0007	18:54:34.8	+00:11:04	PN	
18524+0544	18:54:54.1	+05:48:11	No counterpart	PN[9]
18533+0523	18:55:46.7	+05:27:03	No counterpart	Post-AGB[9]
18576+0341	19:00:11.2	+03:45:46	No counterpart	LBV[10]
18582+0001	19:00:49.0	+00:06:14	Post-AGB	
19016−2330	19:04:43.6	−23:26:09	Transition	
19024+0044	19:05:02.1	+00:48:51	Post-AGB	
19083+0119	19:10:54.5	+01:24:45	No counterpart	Post-AGB[6]
19114+0002	19:13:58.6	+00:07:32	Post-AGB	
19154+0809	19:17:50.6	+08:15:08	PN	
19200+3457	19:21:55.3	+35:02:55	Post-AGB	
19207+2023	19:22:55.8	+20:28:55	Post-AGB	
19208+1541	19:23:05.9	+15:47:31	No counterpart	IR source
19225+3013	19:24:26.9	+30:19:27	Post-AGB	
19306+1407	19:32:55.1	+14:13:37	Post-AGB	
19356+0754	19:38:02.2	+08:01:34	Post-AGB	
19386+0155	19:41:08.3	+02:02:31	Post-AGB	
19422+1438	19:44:31.7	+14:45:25	Post-AGB	
19454+2920	19:47:24.3	+29:28:12	No counterpart	Post-AGB[6]
19477+2401	19:49:54.9	+24:08:53	Post-AGB	
19500−1709	19:52:52.7	−17:01:50	Post-AGB	
19589+4020	20:00:43.0	+40:29:10	Post-AGB	
19589+3419	20:00:52.9	+34:28:22	PN	
19590−1249	20:01:49.8	−12:41:18	Transition	
20160+2734	20:18:05.9	+27:44:04	Post-AGB	
20174+3222	20:19:27.8	+32:32:15	No counterpart	Post-AGB[9]
20259+4206	20:27:42.3	+42:16:44	Post-AGB	
20406+2953	20:42:46.0	+30:04:06	No counterpart	PN cand.[7], post-AGB[9]
20462+3416	20:48:16.6	+34:27:24	Transition	
20572+4919	20:58:55.6	+49:31:13	Post-AGB	
21289+5815	21:30:22.8	+58:28:52	Post-AGB	
21537+6435	21:55:04.5	+64:49:54	No counterpart	Post-AGB[9]
21546+4721	21:56:33.0	+47:36:13	Transition	
22023+5249	22:05:30.3	+53:21:33	Transition	
22036+5306	22:05:30.3	+53:21:33	Post-AGB	
22223+4327	22:24:31.4	+43:43:11	Post-AGB	

[1] Te Lintel Hekkert et al. (1991). [2] van de Steene & Pottasch (1995). [3] B type star with forbidden emission lines and variability. [4] Persi et al. (1994). [5] Bronfman et al. (1996). [6] Hu et al. (1993). [7] Kerber et al. (2003). [8] Zijlstra et al. (1989). [9] García-Lario et al. (1997). [10] Luminous blue variable (Ueta et al. 2001).

Table 3. Sources without detectable water maser emission.

IRAS	V_{min}[1] (km s^{-1})	V_{max}[2] (km s^{-1})	rms[3] (Jy)	Date[4]
00509+6623	−107.7	108.1	0.04	2005-May-20
01005+7910	−121.5	94.3	0.09	2004-Dec.-01
	−107.7	108.0	0.08	2005-May-12
	−107.7	108.0	0.06	2005-May-29
01259+6823	−107.8	107.9	0.07	2005-Feb.-22
02143+5852	−107.8	107.9	0.07	2005-Feb.-22
04137+7016	−108.0	107.7	0.07	2004-Dec.-01
04296+3429	−107.8	107.9	0.06	2005-Mar.-13
05089+0459	−107.6	108.1	0.07	2005-May-29
	−147.4	107.7	0.04	2006-Feb.-02
05113+1347	−108.1	107.7	0.05	2006-Jan.-11
05341+0852	−107.6	108.1	0.06	2005-May-29
05381+1012	−107.9	107.8	0.04	2005-Mar.-13
05471+2351	−108.0	107.7	0.05	2005-Feb.-02
05573+3156	−108.1	107.7	0.05	2005-Feb.-02
06499+0145	−124.0	91.7	0.03	2005-Jan.-03
06518−1041	−108.2	107.6	0.03	2005-Jan.-03
06530−0213	−108.0	107.7	0.04	2005-Feb.-02
06556+1623	−108.2	107.5	0.04	2005-Feb.-03
07134+1005	−108.0	107.7	0.04	2005-Mar.-12
07227−1320	−108.1	107.7	0.04	2005-Mar.-12
07253−2001	−108.2	134.6	0.05	2005-Mar.-12
07430+1115	−106.0	109.8	0.03	2005-Feb.-04
	−108.1	107.6	0.04	2005-Mar.-12
08005−2356	−108.1	107.6	0.06	2005-Mar.-12
08187−1905	−108.1	107.6	0.05	2005-Mar.-12
16476−1122	−107.8	108.0	0.04	2006-Jan.-08
16559−2957	−107.9	107.8	0.14	2005-Sep.-11
17074−1845	−108.1	107.6	0.10	2005-Jul.-27
17086−2403	−107.7	108.0	0.06	2006-Jan.-08
17106−3046	−107.7	108.0	0.10	2006-Jan.-08
17195−2710	−107.7	108.0	0.07	2006-Jan.-08
17203−1534	−108.1	107.6	0.10	2005-Jul.-27
17223−2659	−107.7	108.0	0.12	2006-Jan.-08
	−109.3	106.4	0.05	2006-Mar.-12
17253−2831	−107.7	108.0	0.08	2006-Jan.-09
17269−2235	−107.7	108.0	0.13	2006-Jan.-08
	−107.9	107.8	0.04	2006-Mar.-12
17291−2402	−107.7	108.0	0.08	2006-Jan.-08
	−108.4	107.3	0.05	2006-Mar.-12
17317−2743	−107.7	108.0	0.08	2006-Jan.-09
17332−2215	−107.8	107.9	0.05	2006-Feb.-21
17347−3139	−107.8	107.9	0.3	2005-Oct.-21
	−110.3	105.4	0.14	2006-May-06
17364−1238	−107.7	108.0	0.04	2006-Jan.-09
17371−2747	−107.7	108.0	0.08	2006-Jan.-09
17376−2040	−107.6	108.1	0.06	2006-Feb.-21
17381−1616	−107.9	107.8	0.03	2006-Mar.-12
17388−2203	−108.0	107.7	0.05	2006-Apr.-05
17392−3020	−108.0	107.8	0.14	2005-Sep.-11
17395−0841	−107.9	107.8	0.04	2006-Mar.-12
17418−2713	−107.8	107.9	0.08	2006-Feb.-21
17423−1755	−108.0	107.7	0.05	2006-Apr.-05
17436+5003	−107.9	107.8	0.03	2005-Mar.-13
17441−2411	−108.0	107.7	0.08	2006-Apr.-12

Table 3. continued.

IRAS	V_{min} (km s^{-1})	V_{max} (km s^{-1})	rms (Jy)	Date
17456−2037	−108.0	107.7	0.05	2006-Apr.-12
17466−3031	−108.0	107.7	0.14	2006-Apr.-06
17488−1741	−107.8	107.9	0.08	2005-Oct.-15
17514−1555	−107.4	108.3	0.07	2005-Oct.-15
17516−2526	−107.8	107.9	0.10	2005-Oct.-21
17542−0603	−108.0	107.7	0.03	2006-Apr.-05
17576−2653	−107.7	108.1	0.09	2006-Jan.-09
17579−3121	−108.0	107.7	0.15	2006-Apr.-06
17582−2619	−108.0	107.7	0.07	2006-Apr.-12
17597−1442	−108.1	107.6	0.09	2005-Jul.-27
18044−1303	−107.2	108.6	0.10	2005-Oct.-15
18062+2410	−107.8	107.9	0.06	2005-Mar.-13
18075−0924	−108.4	107.3	0.03	2006-Mar.-12
18186−0833	−108.8	107.0	0.03	2006-Mar.-12
18246−1032	−107.9	107.8	0.04	2006-Mar.-29
18276−1431	−108.1	107.6	0.09	2005-Jul.-28
18401−1109	−107.9	107.9	0.04	2006-Mar.-29
18415−2100	−108.0	107.7	0.07	2005-Sep.-11
	−107.9	107.8	0.05	2006-Apr.-12
18420−0512	–84.3	131.4	0.06	2005-Oct.-15
18442−1144	−107.9	107.9	0.04	2006-Mar.-29
18520+0007	–24.1	191.7	0.06	2005-Jun.-23
	−107.8	108.0	0.03	2006-Mar.-06
18524+0544	−108.1	107.6	0.06	2005-Jul.-28
18533+0523	−108.2	107.5	0.07	2005-Jul.-28
18576+0341	−108.2	107.6	0.07	2005-Jul.-28
18582+0001	−161.6	54.2	0.11	2006-Feb.-03
19016−2330	−107.8	107.9	0.09	2006-Mar.-24
19024+0044	−108.1	107.6	0.08	2005-Jun.-23
19083+0119	−107.8	107.9	0.07	2005-Oct.-15
19114+0002	−107.7	108.0	0.06	2006-Mar.-12
19122−0230	−107.8	107.9	0.09	2006-Mar.-24
19154+0809	−105.5	110.2	0.06	2005-Oct.-15
19200+3457	−107.7	108.0	0.06	2005-Mar.-12
19207+2023	−108.0	107.7	0.08	2005-Jul.-28
19208+1541	−108.0	107.7	0.07	2005-Jul.-28
19225+3013	−107.8	107.9	0.06	2004-Oct.-29
	−108.0	107.7	0.08	2005-Jul.-28
	−108.0	107.7	0.10	2005-Aug.-10
19306+1407	−107.9	107.9	0.06	2005-Oct.-21
	−107.9	107.9	0.06	2006-Apr.-23
19356+0754	−108.0	107.8	0.04	2005-Sep.-22
19386+0155	−107.9	107.9	0.05	2006-Apr.-23
19422+1438	−107.6	108.1	0.06	2006-Jan.-29
19454+2920	−103.0	112.8	0.06	2005-Aug.-26
19477+2401	−107.8	108.0	0.05	2006-Apr.-06
19500−1709	−107.8	108.0	0.09	2006-Mar.-24
19589+4020	−107.7	108.0	0.05	2005-Mar.-12
19589+3419	−108.0	107.8	0.08	2005-Aug.-10
19590−1249	−107.9	107.9	0.05	2006-Apr.-23
20160+2734	−107.9	107.8	0.04	2005-Sep.-23
20174+3222	−108.0	107.8	0.08	2005-Jul.-28
20259+4206	−107.7	108.0	0.07	2005-Mar.-12
20406+2953	−108.0	107.7	0.05	2005-Aug.-26
20462+3416	−107.9	107.9	0.10	2005-Jun.-23

Table 3. continued.

IRAS	V_{min} (km s^{-1})	V_{max} (km s^{-1})	rms (Jy)	Date
20572+4919	–90.3	125.4	0.04	2005-Oct.-15
21289+5815	–107.8	108.0	0.12	2005-May-29
21537+6435	–110.0	105.8	0.024	2005-Feb.-21
21546+4721	–107.7	108.1	0.03	2005-Feb.-21
22023+5249	–107.8	108.6	0.017	2005-Feb.-26
22036+5306	–107.8	108.0	0.04	2006-Feb.-03
22223+4327	–107.6	108.1	0.04	2005-Mar.-12

[1] Minimum velocity covered by the observed bandwidth. [2] Maximum velocity covered by the observed bandwidth. [3] Noise level, 1σ. [4] Date of observation.